

# Subsurface iceberg melt key to Greenland fjord freshwater budget

T. Moon<sup>1\*</sup>, D. A. Sutherland<sup>2</sup>, D. Carroll<sup>2,6</sup>, D. Felikson<sup>3</sup>, L. Kehrl<sup>4</sup> and F. Straneo<sup>5,7</sup>

**Liquid freshwater fluxes from the Greenland ice sheet affect ocean water properties and circulation on local, regional and basin-wide scales, with associated biosphere effects. The exact impact, however, depends on the volume, timing and location of freshwater releases, which are poorly known. In particular, the transformation of icebergs, which make up roughly 30–50% of the loss of the ice-sheet mass to liquid freshwater, is not well understood. Here we estimate the spatial and temporal distribution of the freshwater flux for the Helheim–Sermilik glacier–fjord system in southeast Greenland using an iceberg-melt model that resolves the subsurface iceberg melt. By estimating seasonal variations in all the freshwater sources, we confirm quantitatively that iceberg melt is the largest annual freshwater source in this system type. We also show that 68–78% of the iceberg melt is released below a depth of 20 m and, seasonally, about 40–100% of that melt is likely to remain at depth, in contrast with the usual model assumptions. Iceberg melt also peaks two months after all the other freshwater sources peak. Our methods provide a framework to assess individual freshwater sources in any tidewater system, and our results are particularly applicable to coastal regions with a high solid-ice discharge in Greenland.**

To assess the effects of Greenland freshwater discharge on the ice sheet, ocean and dependent systems requires knowledge of where and when ocean-bound freshwater is released. A recent study estimated iceberg melt within the ice mélange (icebergs and bergy bits distributed near the glacier terminus) in two Greenland fjords using remotely sensed digital elevation models of the fjord surface<sup>1</sup>. The authors concluded that iceberg melt probably dominated the liquid freshwater discharge in winter, but fell short of evaluating the iceberg-melt contribution with respect to all freshwater sources, the separate iceberg-melt processes and the seasonal evolution and vertical distribution of iceberg melt, which have also been neglected in previous iceberg-melt studies<sup>2,3</sup>. Similarly, recent estimates of liquid freshwater transport cannot separate iceberg melt from other sources<sup>4</sup>. In the absence of better information, iceberg-melt production has been ignored in ocean models<sup>5</sup> or treated as ocean-surface input only<sup>6,7</sup>. When included, it has been handled as time invariant, which reflects no seasonal changes, or the discharge of the solid ice sheet has been instantaneously converted into liquid freshwater, ignoring the iceberg transition<sup>6</sup>. Here we develop a new approach to determine iceberg melt (Methods and Supplementary Methods) and apply it to the Helheim–Sermilik glacier–fjord system (Fig. 1), one of the highest discharge systems of solid ice in Greenland. We fully resolve the timing and distribution of the liquid freshwater flux into the fjord, partitioned by source, and elucidate the dominant and spatiotemporally unique role of iceberg melt.

Greenland fjord liquid freshwater flux is composed of terrestrial runoff, subglacial discharge (primarily derived from ice-sheet surface melt), glacier terminus melt and iceberg melt. All of these components feed a cycle of changing fjord water properties and circulation that further modifies ocean waters and influences glacier stability<sup>4,8,9</sup>. For example, the effect of iceberg melt on the vertical and horizontal salinity gradients impacts not only buoyancy-driven

flows but, effectively, all fjord circulation processes (for example, subglacial discharge-driven plumes<sup>10–12</sup>, intermediary circulation<sup>13,14</sup> and internal waves<sup>15,16</sup>). Thus, iceberg-melt-induced changes in the fjord are expected to influence the magnitude, timing and spatial distribution of the submarine melt at glacier termini—a potential trigger of glacier retreat and ice loss<sup>17–19</sup>. Resolving iceberg melt and its spatiotemporal distribution can improve understanding of these associated ice and ocean responses, as well as biosphere effects<sup>20,21</sup>.

Seasonal environmental conditions control most freshwater-flux processes (Fig. 2). Summer snowmelt and precipitation over land create terrestrial runoff, whereas ice-sheet surface snowmelt, ice melt and precipitation create an active glacier hydrological system. This hydrological system facilitates seasonal subglacial discharge, which increases the submarine glacier terminus melt from upwelling meltwater plumes<sup>9,22</sup>. In winter, glacier hydrology shuts down as surface melt ceases, which decreases the subglacial discharge to that produced only through frictional heating and leaves primarily ambient melt at the terminus<sup>23,24</sup>.

Additional fjord conditions influence iceberg melt (Figs. 1 and 2). In the Sermilik Fjord, summer ice cover is concentrated in the near-terminus mélange region (within ~20–30 km from the terminus) (Fig. 1a), with mostly open water elsewhere. Despite a greater sea ice cover in winter<sup>25</sup> (Fig. 1b), Sermilik Fjord is rarely completely ice covered<sup>26</sup> (Supplementary Fig. 1) and strong katabatic down-fjord and cross-fjord winds<sup>27,28</sup> can produce larger winter waves, which potentially enhance wave-induced iceberg melt. However, this effect, and melt along the full iceberg keel depth, is also influenced by seasonally variable fjord stratification; the winter water column is more strongly stratified, with a cold fresh upper layer and a warm, more-saline deep-Atlantic water layer (below ~170 m). Summer has warmer near-surface ocean temperatures and an upper mixed layer<sup>29,30</sup> (Figs. 2 and 3b).

<sup>1</sup>National Snow and Ice Data Center, Cooperative Institute for Research in Environmental Sciences, University of Colorado, Boulder, CO, USA. <sup>2</sup>Department of Earth Sciences, University of Oregon, Eugene, OR, USA. <sup>3</sup>Institute for Geophysics, University of Texas at Austin, Austin, TX, USA. <sup>4</sup>Polar Science Center, Applied Physics Lab and Department of Earth & Space Sciences, University of Washington, Seattle, WA, USA. <sup>5</sup>Dept. of Physical Oceanography, Woods Hole Oceanographic Institution, Woods Hole, MA, USA. Present addresses: <sup>6</sup>Jet Propulsion Laboratory, California Institute of Technology, Pasadena, CA, USA. <sup>7</sup>Scripps Institution of Oceanography, University of California, San Diego, CA, USA. \*e-mail: [twila.science@gmail.com](mailto:twila.science@gmail.com)

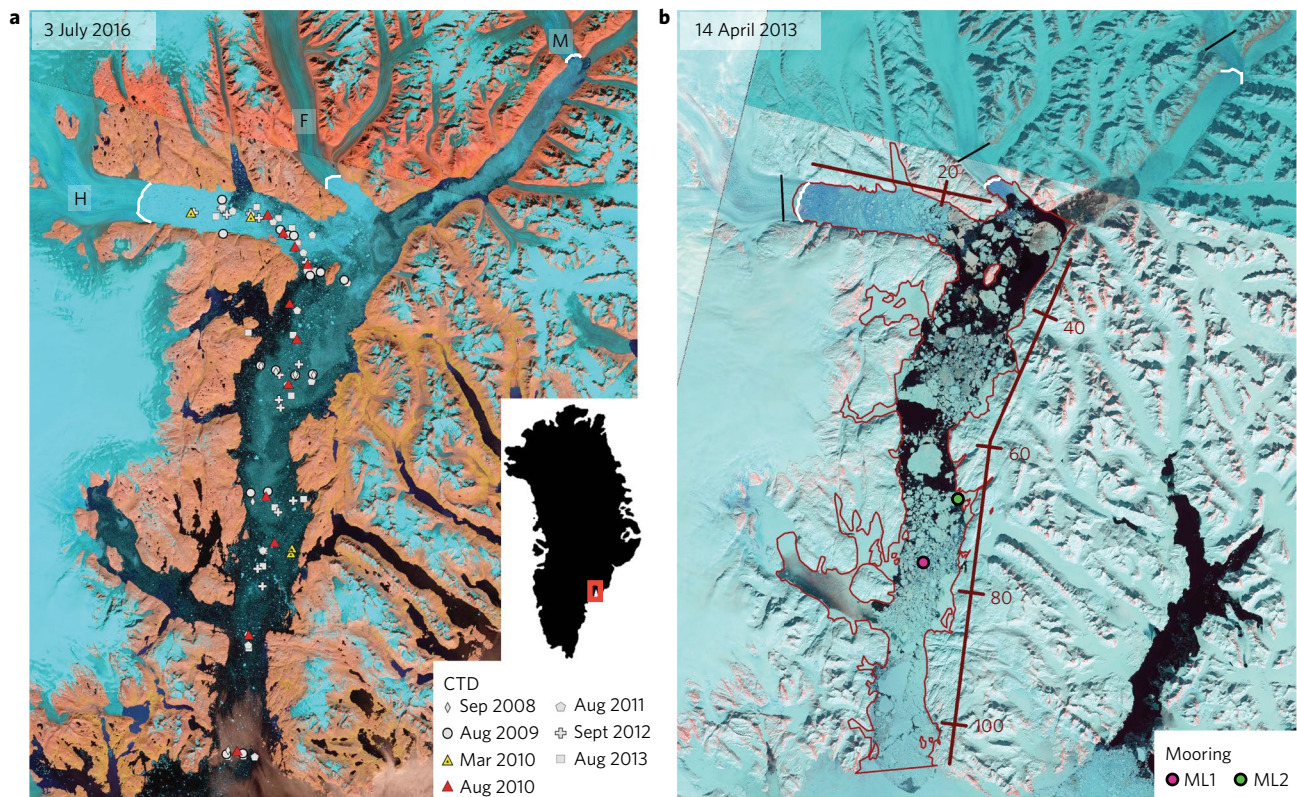


**Fig. 1 | Helheim Glacier and Sermilik Fjord study region. a**, Landsat 8 satellite image of representative summer fjord conditions that shows the locations for Helheim (H), Midgaard (M) and Fenris (F) glaciers, terminus positions (white) and sites of in situ CTD casts. **b**, Representative winter Landsat 8 image with locations of glacier ice discharge flux gates (black lines), terminus positions (white) and in situ ocean moorings ML1 and ML2. The red outline shows the region used for iceberg remote sensing and full fjord freshwater calculations.

### Resolving subsurface iceberg melt

The first goal of this research was to resolve iceberg melt spatially through the vertical water column. To do this, we created an iceberg-melt model (10 m vertical resolution (Supplementary Methods and Supplementary Fig. 2)<sup>2,31,32</sup> to calculate freshwater flux for individual icebergs (50–1,000 m length, 48–393 m keel depth). The model input incorporates in situ ocean temperature, salinity and velocity profiles from CTD (conductivity/temperature/depth) casts<sup>4</sup> and moorings<sup>28</sup>, modelled vertical melt-driven buoyant plume velocities<sup>22</sup>, ERA-Interim global atmospheric reanalysis data<sup>33</sup> and remotely sensed iceberg lengths<sup>26</sup> (Fig. 1 and Supplementary Figs. 3–5). The model includes five key iceberg-melt processes: wave erosion ( $M_{\text{wave}}$ ), forced ( $M_{\text{ta}}$ ) and free ( $M_{\text{ra}}$ ) convection in air and depth-dependent forced ( $M_{\text{tw}}$ ) and free ( $M_{\text{fw}}$ ) convection in water (Fig. 3a and Supplementary Methods). We use CTD casts and moorings to assess the oceanographic conditions, create iceberg-melt calculations from CTD-collected data (Fig. 4) and develop a full annual hydrographic profile from mooring and CTD data (Supplementary Fig. 3), which is used to assess intra-annual freshwater source partitioning (discussed later).

Our in situ CTD-coincident observations from March and August 2010 (Fig. 3b) are representative of the mean conditions during winter (March) and summer (August) (Supplementary Methods) and provide insight into seasonal differences in iceberg melt (Fig. 3c). Above and at the ocean surface, higher summer sea-surface and air temperatures and lower sea-ice concentrations increase surface melt rates by a factor of more than three compared with winter (summer,  $0.90 \text{ m d}^{-1}$ ; winter,  $0.26 \text{ m d}^{-1}$ ). Wave-induced melt generates the highest local melt rates (winter:  $0\text{--}2.2 \text{ m d}^{-1}$ , summer:  $1.7\text{--}4.9 \text{ m d}^{-1}$  (Supplementary Fig. 6 and

Supplementary Table 1). Its limited area of influence (for example, Fig. 3a), however, makes it a minor contributor to total iceberg melt, although it may play an important secondary role by facilitating mechanical iceberg break-up through wave-notch creation<sup>34</sup> (illustrated in Fig. 3a). Below the ocean surface, melting is controlled by water velocity, temperature and stratification, all of which change seasonally. Summer submarine iceberg-melt maxima at  $\sim 100$  and  $\sim 300$  m depth are generated by opposing water velocity directions with a velocity shear zone at  $\sim 170$  m depth. In winter, the velocity shear increases (Supplementary Fig. 5) but the upper water temperatures are colder (Fig. 3b). The result is a reduced melt above the velocity shear zone (responding primarily to colder temperatures) but a greater melt below (responding primarily to higher velocities). The keel depth determines how much an iceberg extends into the deep-water layer, and thus how much the velocity of the deep-water layer opposes the force of the upper water layer on the iceberg and changes the relative velocity of water felt along the iceberg draft<sup>35</sup>. As the keel depth increases below the shear zone, the upper-layer melt rates increase as deeper layer melt rates decrease (Fig. 3c).

### Iceberg melt for the full fjord

To calculate the iceberg-meltwater flux for the entire fjord, we scale up our iceberg-melt model using iceberg size distributions from Landsat 8 and Moderate Resolution Imaging Spectroradiometer (MODIS) images<sup>26</sup> (Methods and Supplementary Fig. 4). Our analysis does not include the Midgaard fjord arm (Fig. 1b); on average  $\sim 90\%$  of fjord iceberg volume is generated by the Helheim Glacier (Supplementary Fig. 7). We also do not include fjord bergy bits (less than  $\sim 30$  m width), which contribute to the

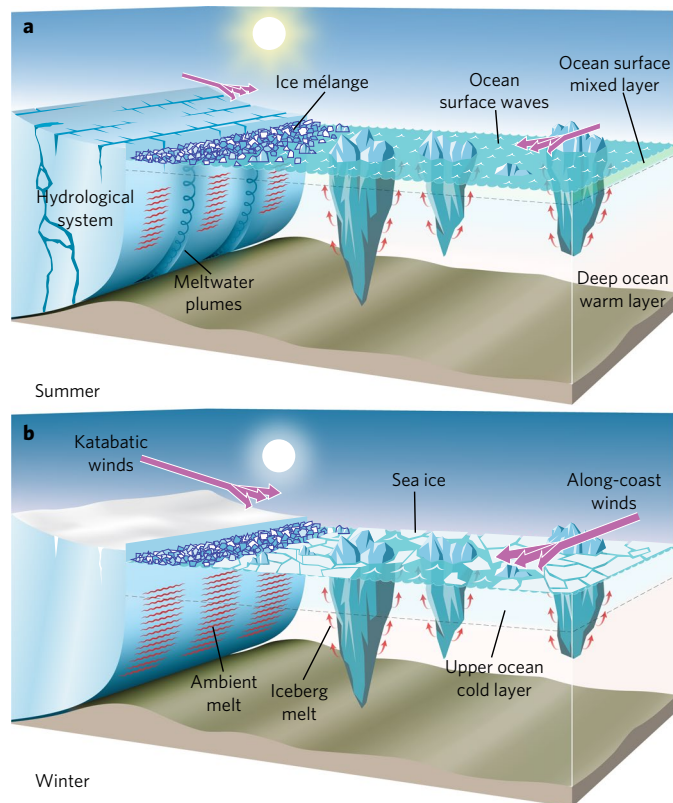


**Fig. 2 | Seasonal differences in the glacier-fjord environment.**

**a,b.** Graphical representation of the glacier-fjord system that highlights the summer (**a**) and winter (**b**) differences. Summer includes an active glacier hydrology system with subglacial discharge driving upwelling plumes at the glacier terminus. Winter includes stronger winds, greater sea-ice extent, diminished solar insolation and differences in vertical ocean temperature and salinity profiles.

surface-layer freshwater flux (shown in Fig. 3d (Supplementary Methods gives bias estimates)). Owing to these two factors, our total iceberg-melt calculations (Fig. 3d,e) represent conservative estimates.

Vertical integration (Fig. 3d) shows that above-water iceberg melt, including wave melt, constitutes 13% (August 2010) to 15% (March 2010) of the total iceberg melt. In contrast, 68–78% (all periods) of the total iceberg melt enters the water column at depths >20 m. Ocean stratification analysis from CTDs indicates a strong summer stratification maximum at 10–20 m depth and a weaker one at 160–170 m depth. In winter, the 10–20 m stratification maximum diminishes, whereas the 160–170 m one remains. Based on ambient plume melt models<sup>11,36</sup>, this density stratification impedes melt upwelling (Methods and Supplementary Fig. 8). As a result, we expect that all the melt produced below 20 m in the summer remains at depth (68–78% below 20 m, including 4–9% below 170 m). In winter, 63% of the melt is produced above 170 m and may ultimately make its way to the surface layer, but 37% is produced, and will probably remain, below 170 m.

Previous research on iceberg melt (and current model standards) input meltwater to near-surface layers<sup>7,37</sup> (for example, the top 6 m grid box<sup>6</sup>), which is clearly problematic given our results. Measurements from the Sermilik Fjord demonstrate that water conditions near the fjord mouth are mirrored by water conditions outside the fjord<sup>30</sup>. This suggests that our vertically partitioned flux from inside the fjord should represent the vertically partitioned flux that leaves the fjord, and can be used directly to better parameterize the freshwater flux for fjord, ocean and ice sheet-ocean modelling.

### Monthly source-partitioned fjord freshwater budget

We complete the fjord freshwater budget by calculating the terrestrial runoff, subglacial discharge and glacier terminus melt (Fig. 4). The runoff of the ice-sheet-surface meltwater within tidewater glacier catchments acts as a proxy for subglacial discharge, and we sample 2008–2015 terrestrial runoff and subglacial discharge from the downscaled 1 km resolution regional atmospheric climate model RACMO2.3 (Methods and ref. <sup>38</sup>). Using these subglacial discharge estimates, we run a terminus-melt model to determine the glacier terminus melt for the Helheim, Midgaard and Fenris Glaciers, and ultimately produce mean annual freshwater fluxes for all the fjord components (Fig. 4).

Flux sources have marked differences in timing and magnitude, which alter their importance throughout the year. Seasonal variations in terminus melt, terrestrial runoff and subglacial discharge are closely tied to atmospheric conditions, which results in similar seasonal timing, but they are differentiated by their peak summer-flux magnitude. Glacierterminus melt may be important for glacier stability, but it is the smallest contributor to freshwater flux (Fig. 4). Ambient melt dominates in winter (Fig. 2b) and our combined Helheim, Midgaard, and Fenris winter melt flux model estimates are  $\sim 16 \text{ m}^3 \text{ s}^{-1}$  (Methods). Summerterminus melt includes ambient melt and melt from subglacial discharge plumes (Fig. 2a), and the three-glacier total peaks at  $\sim 38 \text{ m}^3 \text{ s}^{-1}$  (for ten subglacial conduits (Methods)). Terrestrial runoff is substantially larger than terminus melt, with a mean annual flux of  $\sim 45 \text{ m}^3 \text{ s}^{-1}$  and a summer peak of  $\sim 240 \text{ m}^3 \text{ s}^{-1}$ .

Peak contributions from subglacial discharge are roughly one-to-two orders of magnitude larger than the terrestrial runoff and terminus melt contributions. Despite the small iceberg contributions from the Midgaard and Fenris Glaciers, they produce substantial subglacial discharge (Fig. 4 and Supplementary Fig. 7). Combined with the subglacial discharge from Helheim and two small catchments at mid-fjord, the subglacial discharge is seasonally dominant, and reaches  $\sim 1,800 \text{ m}^3 \text{ s}^{-1}$  at the summer peak (Fig. 4).

For iceberg melt, the first-order link between the melt and ocean temperature and velocity creates a temporal pattern distinct from that of all other sources. The magnitude of the late summer ( $\sim$ August) iceberg-melt flux is roughly half the magnitude of the mid-to-late summer subglacial discharge. As subglacial discharge declines with the melt season, however, iceberg melt increases (primarily in response to warmer ocean waters (Supplementary Fig. 3)) and dominates the monthly freshwater signal for most of the year (Fig. 4). Annually, iceberg melt is also the largest contributor, with a  $\sim 515 \text{ m}^3 \text{ s}^{-1}$  mean annual flux, compared with  $\sim 260 \text{ m}^3 \text{ s}^{-1}$  from subglacial discharge. The actual difference may be even larger, given that recent research suggests RACMO2.3 overestimates runoff<sup>39</sup>, whereas our iceberg-melt estimates are conservative. The spatial fingerprint of iceberg melt is also distinct from other sources that input freshwater only at the fjord boundaries. Together, these results highlight the key role of iceberg melt in the Sermilik Fjord freshwater budget.

Our results align with previous, more-limited estimates of freshwater flux. Using our upper bound of summer submarine terminus melt rates ( $150 \text{ m}^3 \text{ s}^{-1}$ ) and the summer 2013 CTD-coincident iceberg-melt estimate ( $875 \text{ m}^3 \text{ s}^{-1}$ ) yields a total iceberg and terminus flux of  $\sim 1,025 \text{ m}^3 \text{ s}^{-1}$ , at the low end of heat, salt and mass-budget results ( $1,500 \pm 500 \text{ m}^3 \text{ s}^{-1}$ ) (ref. <sup>4</sup>). Focusing only on iceberg melt, summertime (June 2012 and July 2014) calculations of the iceberg-meltwater flux in the mélange region (0–20 km from the terminus) based on digital elevation models yield  $120\text{--}490 \text{ m}^3 \text{ s}^{-1}$  (ref. <sup>1</sup>). Our CTD-coincident summertime fjord-wide iceberg-melt estimates yield  $675\text{--}875 \text{ m}^3 \text{ s}^{-1}$  (using 2012–2014 data only). Estimating that the mélange region constitutes 30–40% of the total fjord iceberg melt, we calculate that its contribution is  $\sim 200\text{--}350 \text{ m}^3 \text{ s}^{-1}$ , within the range of previous mélange-only

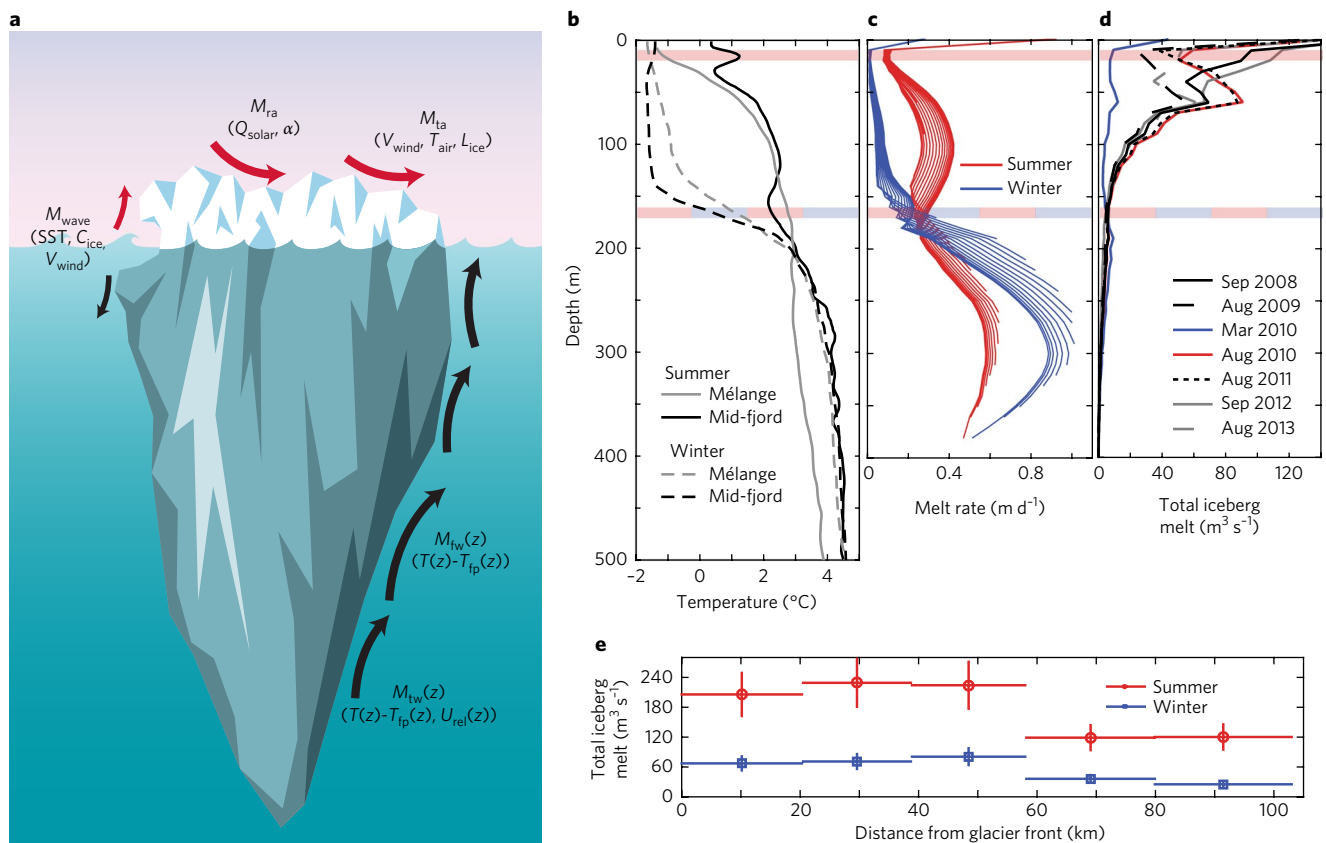


**Fig. 3 | Iceberg melt mechanisms, seasonal oceanographic conditions, and individual and full fjord iceberg melt.** **a**, Iceberg-model melt mechanisms and their environmental dependencies (see Supplementary Table 2 for details) (iceberg vertically exaggerated). **b**, August 2010 (summer) and March 2010 (winter) vertical ocean-temperature profiles for near-glacier mélangé (0–20 km) and mid-fjord (60–80 km). **c**, Modelled vertical summer and winter melt rates for individual icebergs with length  $L = 50$ –1,000 m. **d**, Vertical profiles of total fjord iceberg melt, coincident with CTD measurements. The summer stratification maximum at 10–20 m depth (pink bar) and summer and winter stratification maximum at 160–170 m depth (pink and blue bar) are shown in **b–d**. **e**, Integrated along-fjord summer and winter iceberg melt.

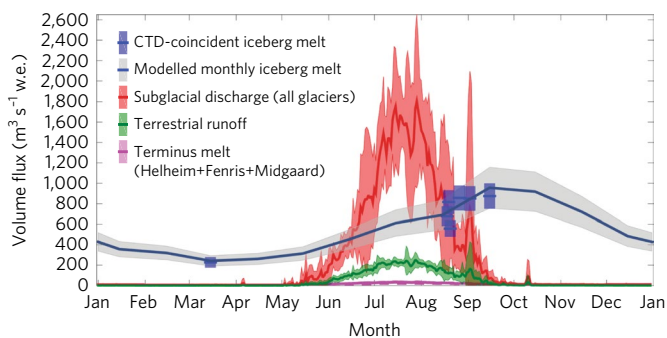


**Fig. 4 | Intra-annual liquid freshwater flux partitioned by source.** Estimated intra-annual freshwater flux for the full Sermilik Fjord. Modelled monthly iceberg melt ( $\text{m}^3 \text{s}^{-1}$  water equivalent) using mean monthly climate and oceanographic data (Methods) and CTD-coincident iceberg melt calculations are shown. Shading for the iceberg melt shows  $\pm 21\%$  based on uncertainty estimates (Methods). Subglacial discharge, terrestrial runoff and terminus melt are the 2008–2015 mean, with one standard deviation shown for subglacial discharge and terrestrial runoff (shaded region) and a terminus melt range based on 1–10 subglacial conduits.

estimates<sup>1</sup>. With our unique method, we then also provide the spatiotemporal resolution needed to incorporate our results into ice sheet and ocean models.

Using our monthly iceberg-melt calculations, we can also explore the transport of solid ice out of the fjord. Based on our solid-ice discharge ( $D$ ) (Supplementary Fig. 7) and iceberg melt ( $M$ ) (Fig. 4), and remotely sensed measurements of the change in total iceberg volume in the fjord over time ( $\frac{dV}{dt}$ ) (ref. <sup>26</sup>), we calculate ice-volume flux out of the fjord ( $Q_{\text{out}}$ ) as:

$$Q_{\text{out}} = D - M - \frac{dV}{dt} \quad (1)$$

Applying a constant ice discharge of  $2.3 \text{ km}^3 \text{ month}^{-1}$  ( $\sim 900 \text{ m}^3 \text{ s}^{-1}$ ) (Supplementary Fig. 7) for time-varying ice discharge based on velocity-flux gates and the mean iceberg melt during July–August, August–September and September–October (time periods based on  $\frac{dV}{dt}$  availability), we find that 52% ( $1.2 \text{ km}^3 \text{ month}^{-1}$ ), 52% ( $1.2 \text{ km}^3 \text{ month}^{-1}$ ) and 22% ( $0.5 \text{ km}^3 \text{ month}^{-1}$ ), respectively, of solid-ice discharge exits the fjord. The result is a substantial subsurface freshening from summer into autumn and a decrease in iceberg transport from the fjord. Combining our melt-flux methods with future improvements in time-varying solid-ice discharge (including terminus advance and retreat) and fjord ice volume measurements will facilitate more-detailed time series of solid-ice transport.

Our analysis provides conclusive evidence that iceberg melt is the largest fjord freshwater contributor for this major glacier–fjord system and that its temporal, horizontal and vertical distribution is distinct from that of all other sources. As the dominant freshwater source for the Sermilik Fjord, it cannot be ignored for this

system. Although our new framework to assess the complete liquid freshwater budget is applicable to all tidewater glacier systems, our results are most-directly transferrable to coastal regions near high-discharge Greenland glaciers, such as Jakobshavn Isbrae, Kangerdlugssuaq Glacier and other fast-flowing glaciers<sup>40</sup>. As the top producers of solid ice-discharge, these areas are the most important for understanding the future dynamic mass loss of ice, and our results indicate that iceberg melt must be a part of this analysis. Similarities in fjord stratification around the ice sheet<sup>16</sup> help transfer our results to other Greenland regions. Substantial heterogeneity in the ice-sheet-wide distribution of ice loss via surface mass balance versus solid-ice discharge<sup>41</sup> also suggests that iceberg melt may be locally or regionally dominant, particularly for regions along the northwest and southeast coasts where the majority of fast-flowing Greenland tidewater glaciers are located<sup>42</sup> and solid-ice discharge is large. Iceberg mobility and residence time, which depend on ocean and atmospheric conditions, also influence local iceberg-melt fluxes, which potentially increases the importance of iceberg melt within systems with lower rates of solid-ice discharge but long iceberg-residence times. Given that icebergs account for ~30–50% of Greenland mass loss<sup>40,43,44</sup>, there is no doubt that understanding their solid-to-liquid transition is important on an ice-sheet-wide scale. The results presented here provide a step-change improvement for current research efforts, and combining our methods with current efforts to increase in situ ocean data<sup>45</sup> and analyse pan-Greenland iceberg distribution and motion<sup>46</sup> will facilitate future spatiotemporal analysis of the iceberg freshwater flux for the entire ice sheet. Assessing the spatiotemporal signal of individual freshwater sources, as we have done here, can also improve model parameterizations. To resolve the sources, timing and input locations of freshwater is critical for projecting the impacts of surface mass balance and ice-discharge changes<sup>47,48</sup> on both the ice sheet and the ocean.

## Methods

Methods, including statements of data availability and any associated accession codes and references, are available at <https://doi.org/10.1038/s41561-017-0018-z>.

Received: 11 July 2017; Accepted: 3 November 2017;  
Published online: 4 December 2017

## References

- Enderlin, E. M., Hamilton, G. S., Straneo, F. & Sutherland, D. A. Iceberg meltwater fluxes dominate the freshwater budget in Greenland's iceberg-congested glacial fjords. *Geophys. Res. Lett.* **43**, 287–294 (2016).
- Bigg, G. R., Wadley, M. R., Stevens, D. P. & Johnson, J. A. Modelling the dynamics and thermodynamics of icebergs. *Cold Reg. Sci. Tech.* **26**, 113–135 (1997).
- Hill, J. C. & Condron, A. Subtropical iceberg scours and meltwater routing in the deglacial western North Atlantic. *Nat. Geosci.* **7**, 806–810 (2014).
- Jackson, R. H. & Straneo, F. Heat, salt, and freshwater budgets for a glacial fjord in Greenland. *J. Phys. Oceanogr.* **46**, 2735–2768 (2016).
- Luo, H. et al. Oceanic transport of surface meltwater from the southern Greenland ice sheet. *Nat. Geosci.* **9**, 528–532 (2016).
- Böning, C. W., Behrens, E., Biastoch, A., Getzlaff, K. & Bamber, J. L. Emerging impact of Greenland meltwater on deepwater formation in the North Atlantic Ocean. *Nat. Geosci.* **9**, 523–527 (2016).
- Gillard, L. C., Hu, X., Myers, P. G. & Bamber, J. L. Meltwater pathways from marine terminating glaciers of the Greenland Ice Sheet. *Geophys. Res. Lett.* **43**, 10873–10882 (2016).
- Mortensen, J., Lennert, K., Bendtsen, J. & Rysgaard, S. Heat sources for glacial melt in a sub-Arctic fjord (Godthåbsfjord) in contact with the Greenland Ice Sheet. *J. Geophys. Res.* **116**, C006528 (2011).
- Carroll, D. et al. Modeling turbulent subglacial meltwater plumes: implications for fjord-scale buoyancy-driven circulation. *J. Phys. Oceanogr.* **45**, 2169–2185 (2015).
- Sciascia, R., Straneo, F., Cenedese, C. & Heimbach, P. Seasonal variability of submarine melt rate and circulation in an East Greenland fjord. *J. Geophys. Res. Oceans* **118**, 2492–2506 (2013).
- Carroll, D. et al. The impact of glacier geometry on meltwater plume structure and submarine melt in Greenland fjords. *Geophys. Res. Lett.* **43**, 9739–9748 (2016).
- Xu, Y., Rignot, E., Fenty, I., Menemenlis, D. & Mar Flexas, M. Subaqueous melting of Store Glacier, West Greenland from three-dimensional, high-resolution numerical modeling and ocean observations. *Geophys. Res. Lett.* **40**, 4648–4653 (2013).
- Inall, M. E. et al. Oceanic heat delivery via Kangerdlugssuaq Fjord to the south-east Greenland ice sheet. *J. Geophys. Res. Oceans* **119**, 631–645 (2014).
- Klinck, J. M., O'Brien, J. J. & Svendsen, H. A simple model of fjord and coastal circulation interaction. *J. Phys. Oceanogr.* **11**, 1612–1626 (1981).
- Arneborg, L. Turnover times for the water above sill level in Gullmar Fjord. *Continental Shelf Res.* **24**, 443–460 (2004).
- Straneo, F. & Cenedese, C. The dynamics of Greenland's glacial fjords and their role in climate. *Annu. Rev. Marine Sci* **7**, 89–112 (2015).
- Cook, A. J. et al. Ocean forcing of glacier retreat in the western Antarctic Peninsula. *Science* **353**, 283–286 (2016).
- Motyka, R. J. et al. Submarine melting of the 1985 Jakobshavn Isbrae floating tongue and the triggering of the current retreat. *J. Geophys. Res.* **116**, F01007 (2011).
- Holland, D. M., Thomas, R. H., De Young, B., Ribergaard, M. H. & Lyberth, B. Acceleration of Jakobshavn Isbrae triggered by warm subsurface ocean waters. *Nat. Geosci.* **1**, 659–664 (2008).
- Bhatia, M. P. et al. Greenland meltwater as a significant and potentially bioavailable source of iron to the ocean. *Nat. Geosci.* **6**, 274–278 (2013).
- Arendt, K. E., Agersted, M. D., Sejir, M. K. & Juul-Pedersen, T. Glacial meltwater influences on plankton community structure and the importance of top-down control (of primary production) in a NE Greenland fjord. *Estuarine Coastal Shelf Sci.* **183**, 123–135 (2016).
- Jenkins, A. Convection-driven melting near the grounding lines of ice shelves and tidewater glaciers. *J. Phys. Oceanogr.* **41**, 2279–2294 (2011).
- Fried, M. J., Catania, G. A. & Bartholomaeus, T. C. Distributed subglacial discharge drives significant submarine melt at a Greenland tidewater glacier. *Geophys. Res. Lett.* **42**, 9328–9336 (2015).
- Christoffersen, P., O'Leary, M. & Van Angelen, J. H. & Van den Broeke, M. Partitioning effects from ocean and atmosphere on the calving stability of Kangerdlugssuaq Glacier, East Greenland. *Ann. Glaciol.* **53**, 249–256 (2012).
- Andres, M., Silvano, A., Straneo, F. & Watts, D. R. Icebergs and sea ice detected with inverted echo sounders. *J. Atmos. Oceanic Technol.* **32**, 1042–1057 (2015).
- Sulak, D. J., Sutherland, D. A. & Enderlin, E. M. Iceberg properties and distributions in three Greenlandic fjords using satellite imagery. *Ann. Glaciol.* **1–15** (2017).
- Oltmanns, M., Straneo, F., Moore, G. W. K. & Mernild, S. H. Strong downslope wind events in Ammassalik, SE Greenland. *J. Climate* **37**, 977–993 (2013).
- Straneo, F., Hamilton, G. S., Stearns, L. A. & Sutherland, D. A. Connecting the Greenland Ice Sheet and the ocean: a case study of Helheim Glacier and Sermilik Fjord. *Oceanography* **29**, 34–45 (2016).
- Sutherland, D. A., Straneo, F. & Pickart, R. S. Characteristics and dynamics of two major Greenland glacial fjords. *J. Geophys. Res. Oceans* **119**, 3767–3791 (2014).
- Straneo, F. et al. Rapid circulation of warm subtropical waters in a major glacial fjord in East Greenland. *Nat. Geosci.* **3**, 182–187 (2010).
- Silva, T. A. M., Bigg, G. R. & Nicholls, K. W. Contribution of giant icebergs to the Southern Ocean freshwater flux. *J. Geophys. Res.* **111**, C03004–C03008 (2006).
- Savage, S. B. in *Geomorphological Fluid Mechanics* (eds Balmforth, N. J. & Provenzale, A.) 279–318 (Lecture Notes in Physics 582, Springer, Heidelberg, 2001).
- Dee, D. P. et al. The ERA-Interim reanalysis: configuration and performance of the data assimilation system. *Q. J. R. Meteorol. Soc.* **137**, 553–597 (2011).
- Wagner, T., Wadhams, P. & Bates, R. The 'footloose' mechanism: iceberg decay from hydrostatic stresses. *Geophys. Res. Lett.* **41**, 5522–5529 (2014).
- FitzMaurice, A., Straneo, F., Cenedese, C. & Andres, M. Effect of a sheared flow on iceberg motion and melting. *Geophys. Res. Lett.* **43**, 12520–12527 (2016).
- Jenkins, A. in *Ice in the Climate System Mechanics* (ed. Peltier, W. R.) 217–235 (NATO ASI Series 12, Springer, Heidelberg, 1993).
- Wilton, D. J., Bigg, G. R. & Hanna, E. Modelling twentieth century global ocean circulation and iceberg flux at 48°N: implications for west Greenland iceberg discharge. *Prog. Oceanogr.* **138**, 194–210 (2015).
- Noël, B. et al. A daily, 1 km resolution data set of downscaled Greenland ice sheet surface mass balance (1958–2015). *Cryosphere* **10**, 2361–2377 (2016).
- Smith, L. C. et al. Direct measurements of meltwater runoff on the Greenland Ice Sheet surface. *Proc. Natl Acad. Sci. USA* <http://doi.org/10.1073/pnas.1707743114> (in the press).
- Enderlin, E. M. et al. An improved mass budget for the Greenland Ice Sheet. *Geophys. Res. Lett.* **41**, 866–872 (2014).

41. Kjeldsen, K. K. et al. Spatial and temporal distribution of mass loss from the Greenland Ice Sheet since AD 1900. *Nature* **528**, 396–400 (2015).
42. Moon, T., Joughin, I., Smith, B. & Howat, I. 21st-century evolution of Greenland outlet glacier velocities. *Science* **336**, 576–578 (2012).
43. Bamber, J., Van Den Broeke, M., Ettema, J., Lenaerts, J. & Rignot, E. Recent large increases in freshwater fluxes from Greenland into the North Atlantic. *Geophys. Res. Lett.* **39**, L19501 (2012).
44. van den Broeke, M. R. et al. On the recent contribution of the Greenland ice sheet to sea level change. *Cryosphere* **10**, 1933–1946 (2016).
45. Fenty, I. et al. Oceans melting Greenland: early results from NASA's ocean-ice mission in Greenland. *Oceanography* **29**, 72–83 (2016).
46. Stearns, L. A. et al. Quantification of calving rates and iceberg size distribution in West Greenland. In *2016 Ocean Sci. Meeting* (AGU, ASLO, TOS, New Orleans, 2016).
47. Fyke, J. G., Vizcaino, M., Lipscomb, W. & Price, S. Future climate warming increases Greenland ice sheet surface mass balance variability. *Geophys. Res. Lett.* **41**, 470–475 (2014).
48. Fürst, J. J., Goelzer, H. & Huybrechts, P. Ice-dynamic projections of the Greenland ice sheet in response to atmospheric and oceanic warming. *Cryosphere* **9**, 1039–1062 (2015).

### Acknowledgements

We thank M. van den Broeke and B. Noël for downscaled RACMO2.3 data, I. Joughin for TerraSAR-X ice-velocity data through the NASA-funded MEaSUREs Program (NNX13AI21A) and S. Powell for illustrations. T.M. was in part supported by National

Science Foundation (NSF) Ocean Sciences (OCE) 1420096. D.A.S. was partially supported by NSF grant 1552232. L.K. was supported by a National Defense Science & Engineering Graduate Fellowship. F.S. was supported by NSF PLR 1418256 and OCE 1434041. Synthesis of the Sermilik Fjord data was supported by EarthCube GRISO RCN NSF ICER 1541390.

### Author contributions

T.M. and D.A.S. designed the study and led the analysis and writing. L.K. contributed glacier discharge data and analysis, D.F. contributed hydrology-catchment basins and data sampling, D.C. modelled buoyant plumes and terminus melt, and F.S. contributed oceanographic data and interpretation. All of the authors contributed to the final manuscript.

### Competing interests

The authors declare no competing financial interests.

### Additional information

**Supplementary information** is available for this paper at <https://doi.org/10.1038/s41561-017-0018-z>.

**Reprints and permissions information** is available at [www.nature.com/reprints](http://www.nature.com/reprints).

**Correspondence and requests for materials** should be addressed to T.M.

**Publisher's note:** Springer Nature remains neutral with regard to jurisdictional claims in published maps and institutional affiliations.

## Methods

**Iceberg-melt model.** To calculate iceberg melt, we developed an individual iceberg-melt model, which is explained in depth in Supplementary Information. Key concepts and references (Supplementary Methods gives additional details) used in the iceberg-melt model are summarized here:

- We test icebergs of length  $L$  (longest axis at the waterline) 50–1,000 m, and develop a geometry for icebergs of keel depth less than 200 m from ref. <sup>49</sup>. The shortest waterline axis width,  $W$ , equals  $L/1.62$  (ref. <sup>50</sup>). The width is modified to make the iceberg stable for the four smallest-size classes based on ref. <sup>51</sup>. We do not allow icebergs to roll<sup>52,53</sup> or overhanging slabs to fracture and calve off icebergs<sup>52,54</sup>.
- To model the five iceberg-melt processes included—wave erosion ( $M_{\text{wave}}$ ), forced ( $M_{\text{fa}}$ ) and free ( $M_{\text{fw}}$ ) convection in air, and depth-dependent forced ( $M_{\text{fw}}$ ) and free ( $M_{\text{fw}}$ ) convection in water—we use parameterizations developed in previous studies and tuned for use in operational iceberg models<sup>51</sup>.
- Supplementary Methods contains a discussion of the uncertainties in iceberg-melt estimates, including a table that assesses uncertainties arising from differences in methods, atmospheric conditions and parameter choices.

**Model input data.** Supplementary Methods also includes details on the model input data, which include:

- Hydrographic data from six summertime research cruises (2008–2013) and one wintertime survey conducted by helicopter and a small boat during March 2010<sup>29</sup>.
- Time series of hydrographic observations from mid-fjord moorings that were installed in 2009<sup>1</sup> (Fig. 1b).
- Observations of water velocities from an upward-looking acoustic Doppler current profiler (ADCP)<sup>54</sup>.
- Vertical water velocities estimated using two methods: (1) a commonly used one-dimensional buoyant-plume model<sup>22</sup> and (2) idealized numerical experiments with an ice–ocean coupled MITgcm (Massachusetts Institute of Technology General Circulation Model) simulation<sup>55</sup>.
- Wind speed, 2 m air temperature and net downward-radiation flux from the ERA-Interim reanalysis project<sup>33</sup>.
- Sea-ice cover based on the analysis of Landsat 8 and MODIS imagery<sup>26</sup> and observations at Sermilik Fjord<sup>25</sup>.

**Estimates of total fjord iceberg melt.** Once we have mean melt rates for each iceberg-size class over each set of environmental conditions, we can calculate a melt flux from the icebergs. We then use these melt fluxes for each iceberg-size class, along with the observed iceberg distributions, to estimate the total melt flux from icebergs into the fjord.

The first step is to take the melt rates (metres per day) and calculate melt fluxes (cubic metres per second) for each melt process (Fig. 2a). To do so, we multiply each melt rate by an appropriate surface area to derive the melt flux. For  $M_{\text{wave}}$ , we assume the iceberg is travelling obliquely into the waves, so that wave erosion only effectively drives melt along one length and one width. Also,  $M_{\text{wave}}$  only affects a vertical extent equal to twice its wave height ( $H_{\text{wave}}$ ), but split between one above the water layer and one below the water layer. Thus, the melt flux caused by  $M_{\text{wave}}$  is applied to an area equal to  $(LH_{\text{wave}} + WH_{\text{wave}}) + (LH_{\text{wave}} + W_{\text{uw},1}H_{\text{wave}})$ , where  $L_{\text{uw},1}$  and  $W_{\text{uw},1}$  are the length and width, respectively, of the first iceberg layer underwater and  $H_{\text{wave}}$  is the wave height driven by winds (Supplementary Table 2 gives parameter symbols, descriptions and their applied range and/or definition). The smaller area affected by  $M_{\text{wave}}$  results in melt fluxes similar in magnitude to other terms, despite the much larger melt-rate magnitudes (Supplementary Fig. 6 and Supplementary Table 1). For  $M_{\text{fa}}$ , the melt flux is calculated using the planar surface area of the above water portion of the iceberg, or  $LW$ . For  $M_{\text{fb}}$ , we assume the wind acts on three sides of the iceberg above water (that is, all except the lee side), as well as on one-half of the surface of the above-water iceberg area. Thus, the melt flux for  $M_{\text{fa}}$  is calculated using an area equal to  $(2LH + WH) + 0.5(LW)$ . For the buoyancy-convection driven melt,  $M_{\text{fw}}$ , the melt flux is calculated using the depth-dependent melt at each layer multiplied by the layer area on all submerged sides, equal to  $(2dzL + 2dzW)$  and summed over each  $z_n$  layer below water. Finally, the melt flux for turbulent convection,  $M_{\text{fw}}$ , is calculated similarly to  $M_{\text{fw}}$ , but only along three sides of the iceberg, assuming there is a lee side not affected by water motion, akin to  $M_{\text{fa}}$ . Thus, for each  $z_n$  layer, the area  $M_{\text{fw}}$  is applied to is  $(2dzL + dzW)$  and the total flux is the sum over all of these layers.

Summing these melt fluxes together gives a vertically varying iceberg melt flux for each size class (Fig. 2). To derive the total iceberg-melt flux over the Sermilik Fjord, we then scale these results using observed iceberg distributions from optical satellite imagery<sup>26</sup>. Supplementary Fig. 4 shows the mean distribution of icebergs in the Sermilik Fjord as a function of size class binned by  $L$ . The same data can be used to estimate the along-fjord variation in iceberg distribution, which shows that slight differences arise between zones close to the fjord mouth versus those closer to the glacier termini (Supplementary Fig. 4). For each size class, we multiply the number of icebergs in the size class by the melt flux calculated for that size class and the given forcing. We then sum these contributions to arrive

at a total iceberg-melt flux. We can partition the iceberg-melt flux to show its depth dependence or along-fjord dependence (Fig. 2). We use the same distribution data for summer, winter and seasonal runs of the iceberg-melt model. We justify this approximation for several reasons. First, the Helheim Glacier, the main source of icebergs to the fjord, often calves year round, with minimal regular seasonality observed (Supplementary Fig. 7)<sup>28,56</sup>. Second, the fjord is typically not frozen over with fast ice in the winter<sup>56</sup>, which suggests that icebergs can move around and not accumulate. The latter evidence is further supported by GPS-tracked icebergs that continually move throughout the winter months<sup>59</sup>. Finally, this is a pragmatic choice, given that no data exist on iceberg distributions in the winter months.

**Glacier ice flux.** To compare solid-ice discharge volume from the Helheim, Fenris and Midgaard Glaciers (Supplementary Fig. 7) with the subsequent freshwater flux, we estimate the ice flux across the flux gates shown in Fig. 1b. The ice flux,  $Q$ , is:

$$Q = \int_0^W u(x, t)H(x, t)dx \quad (9)$$

where  $x$  is the coordinate parallel to the flux gate,  $t$  is time,  $W$  is the glacier width,  $u(x, t)$  is the depth-averaged velocity normal to the flux gate and  $H(x, t)$  is the ice thickness. We assume that the depth-averaged velocity is equal to the surface velocity. Given that basal sliding accounts for >90% of the surface velocity under the main trunk of Helheim<sup>57</sup>, the depth-averaged velocity should be within ~2% of the surface velocity<sup>58</sup>. Although less is known about basal sliding at Midgaard and Fenris, surface velocities are >1,000 m yr<sup>-1</sup> at both glaciers, which probably indicates plug flow. We calculate ice flux for all of the time periods with surface-velocity measurements, and the ice-thickness measurements are linearly interpolated to match those time periods. We use glacier-velocity estimates from the speckle tracking of synthetic aperture radar (SAR) images from the TerraSAR-X mission for Helheim and Midgaard<sup>59</sup> and from feature tracking of Landsat 7/8 and ASTER optical imagery for Fenris<sup>60</sup>. To calculate the ice thickness for Helheim, we use point bed-elevation measurements from the Center for Remote Sensing of Ice Sheets (CreSIS) and surface-elevation measurements from Worldview-1/2/3 and TanDEM-X (ref. <sup>38</sup>). Very few bed-elevation measurements exist for Fenris and Midgaard, so we substitute bed elevations inferred from mass continuity for those glaciers<sup>61</sup>. The inferred bed elevations have large uncertainties. At Midgaard, surface-elevation measurements at the flux gate indicate that the glacier thinned below the inferred bed elevation in 2014. As a result, we decreased the bed elevation at the flux gate by 145 m, so that the surface elevation at the flux gate remained above the bed elevation and bed elevations downstream of the flux gate matched radar ice thicknesses collected by CreSIS in 2013. Surface-elevation measurements for Fenris and Midgaard are from National Aeronautics and Space Administration (NASA)'s Airborne Topographic Mapper (ATM)<sup>62</sup>. The ice-flux estimates are converted into a mass flux assuming a constant ice density of  $\rho_i = 900 \text{ kg m}^{-3}$ . Based on the quality of the available data for each glacier, we assume uncertainties of 6%, 20% and 100% in our ice-flux estimates for Helheim, Fenris and Midgaard, respectively. The uncertainty estimates arise from bed-elevation uncertainties of 50 m for Helheim, 100 m for Fenris and 200 m for Midgaard, which we determined by comparing the limited bed-elevation measurements with the BedMachine v2 (ref. <sup>61</sup>). All other uncertainty sources should be comparatively small.

We use the mean flux-gate cross-sectional areas for Helheim, Midgaard and Fenris when converting estimates of the submarine terminus melt to freshwater flux. These are  $4.522 \times 10^6 \text{ m}^2$ ,  $4.4646 \times 10^5 \text{ m}^2$  and  $2.2534 \times 10^6 \text{ m}^2$  for Helheim, Midgaard and Fenris, respectively. These cross-section areas may be overestimates as they are extracted several kilometres up-glacier of each terminus (Fig. 1b), although further evaluation of this question is limited because of bed topography uncertainties.

**Subglacial discharge and terrestrial runoff.** As it is not possible to measure subglacial discharge directly, we use surface runoff as a proxy. We use separate glacier hydrological catchments for Helheim, Fenris, Midgaard and several smaller glaciers to sample regional atmospheric climate model surface runoff data. For the glacier hydrology basins, we delineate glacier catchments using standard watershed analysis and assuming water flows in the direction of the negative of the gradient of the subglacial hydropotential<sup>63</sup> (Supplementary Fig. 7). Ice-sheet-bed topography is defined by the BedMachine v2 bed<sup>61</sup> and the ice surface is defined by the Greenland Ice Mapping Project (GIMP) digital elevation model<sup>64</sup>. We manually group watersheds that contribute to each marine-terminating glacier terminus in a manner similar to that of ref. <sup>65</sup>. These hydrological catchments are used to estimate subglacial discharge into the fjord. All other hydrological catchments are used to estimate terrestrial runoff into the fjord. For each catchment, we extract daily surface runoff data from the 1 km resolution downscaled regional atmospheric climate model RACMO2.3 (ref. <sup>38</sup>) (results in Supplementary Fig. 7). We use the interannual variability in surface runoff about the 2008–2015 mean as a measure of the uncertainty in the runoff estimates during any given year (green and red shading for terrestrial runoff and subglacial discharge, respectively (Fig. 4)). As in previous studies<sup>56</sup>, we assume that within marine-terminating glacier catchments, all the surface melt is discharged as subglacial freshwater, which is a reasonable assumption given no known or observed mechanisms for increasing the net subglacial water storage. We also assume that all the runoff is delivered to the fjord

instantaneously. This assumption may affect the precise timing of subglacial water discharge, but it should have little influence on our monthly scale comparisons of freshwater-flux sources.

**Terminus-melt model.** To estimate the submarine terminus melt from Helheim, Fenris and Midgaard, we combine a point-source subglacial plume model with an ambient line plume model<sup>22</sup>. This model formulation follows the methods described in the supporting information (S1) of ref. <sup>11</sup>. The ambient plume model is used to simulate melt-driven (that is, free) convection in regions outside of the subglacial discharge plumes<sup>66</sup>. We compute monthly and daily climatologies of linearly interpolated hydrographic profiles and subglacial discharge, respectively; these are time stepped and used as input for the plume models. Melt rates are calculated using a three-equation thermodynamic model<sup>67</sup>. We assume that the ambient melt is horizontally uniform across the width of the terminus, except in regions where the subglacial plumes are active. Simulations with one, five and ten subglacial conduits (with the subglacial discharge held fixed) spaced evenly across the width of the terminus are conducted; net submarine terminus-melt fluxes are computed by spatially integrating the submarine melt in the subglacial discharge plume and ambient regions. Increasing the turbulent transfer coefficients in the ambient plume model by a factor of five results in roughly a 444% increase in the mean submarine terminus melt at peak subglacial discharge. We acknowledge that our ambient plume model assumes that submarine melting outside of the subglacial plume region is driven solely by free convection; strong flows generated by external forcing, such as shelf-forced winds<sup>54</sup>, or induced by buoyancy-driven circulation<sup>9</sup>, may result in larger ambient melt rates along the ice front.

We also use our ambient line plume model to examine whether iceberg melt produced at depth remains at depth or rises vertically in the water column and penetrates through strong stratification layers. We test this using four iceberg-size classes ( $d = 76, 166, 239$  and  $392$  m) and both standard turbulent transfer coefficients and standard turbulent transfer coefficients multiplied by a factor of five, which increases melt and hence vertical plume velocity. The results indicate that melt plumes reach neutral buoyancy rapidly, which allows the melt to remain at depth (Supplementary Fig. 8).

**Data availability.** ERA-Interim data are available from the ECMWF website at [www.ecmwf.int/en/research/climate-reanalysis/reanalysis-datasets/era-interim](http://www.ecmwf.int/en/research/climate-reanalysis/reanalysis-datasets/era-interim). Downscaled RACMO2.3 data were provided by M. van den Broeke and are not available publicly. Greenland BedMachine data are available at [sites.uci.edu/morlighem/dataproducts/bedmachine-greenland](http://sites.uci.edu/morlighem/dataproducts/bedmachine-greenland) and GIMP surface elevation data at [nsidc.org/data/docs/measures/nsidc-0645](http://nsidc.org/data/docs/measures/nsidc-0645). Ice-flow velocities derived from Landsat and TerraSAR-X are available at [nsidc.org/data/nsidc-0646](http://nsidc.org/data/nsidc-0646) and [nsidc.org/data/nsidc-0481](http://nsidc.org/data/nsidc-0481) and ATM data at [nsidc.org/data/ILATM2/versions/2](http://nsidc.org/data/ILATM2/versions/2). Iceberg distribution data are available at [www.oceanice.org/icebergs-research](http://www.oceanice.org/icebergs-research) and on request to T.M. Data from fjord moorings, including ADCP data, are available through these URLs (address numbers refer to National Ocean Data Center (NODC) accession number): [accession.nodc.noaa.gov/123217](http://accession.nodc.noaa.gov/123217) (2008–2009), [accession.nodc.noaa.gov/127320](http://accession.nodc.noaa.gov/127320) (2009–2012), [accession.nodc.noaa.gov/123282](http://accession.nodc.noaa.gov/123282) (2010–2011), [accession.nodc.noaa.gov/126772](http://accession.nodc.noaa.gov/126772) (2011–2012) and [accession.nodc.noaa.gov/127325](http://accession.nodc.noaa.gov/127325) (2012–2013). Ocean hydrographic profile data is available upon request to T.M. Requests for data in specific formats or not listed here can be directed to the corresponding author.

**Code availability.** The iceberg and terminus-melt model code is available as a set of MATLAB scripts from the authors.

## References

- Barker, A., Sayed, M., & Carrieres, T. Determination of iceberg draft, mass and cross-sectional areas NRC Publications Archive (NPARC). In *Proc. 14th Int. Offshore Polar Engin. Conf.* 899–904 (National Research Council Canada, Ottawa, 2004).
- Dowdeswell, J. A., Whittington, R. J. & Hodgkins, R. The sizes, frequencies, and freeboards of East Greenland icebergs observed using ship radar and sextant. *J. Geophys. Res.* **97**, 3515–3528 (1992).
- Wagner, T. J. W. & Eisenman, I. How climate model biases skew the distribution of iceberg meltwater. *Geophys. Res. Lett.* **44**, 3691–3699 (2017).
- Weeks, W. F. & Mellor, M. *Some Elements of Iceberg Technology* Technical Report (Cold Regions Research and Engineering Laboratory, Hanover, 1978).
- Burton, J. C. et al. Laboratory investigations of iceberg capsizing dynamics, energy dissipation and tsunamigenesis. *J. Geophys. Res. Earth* **117**, F01007 (2012).
- Jackson, R. H., Straneo, F. & Sutherland, D. A. Externally forced fluctuations in ocean temperature at Greenland glaciers in non-summer months. *Nat. Geosci.* **7**, 503–508 (2014).
- Marshall, J., Adcroft, A., Hill, C., Perelman, L. & Heisey, C. A finite-volume, incompressible Navier Stokes model for studies of the ocean on parallel computers. *J. Geophys. Res.* **102**, 5753–5766 (1997).
- Moon, T. et al. Distinct patterns of seasonal Greenland glacier velocity. *Geophys. Res. Lett.* **41**, 7209–7216 (2014).
- Shapiro, D. R., Joughin, I. R., Poinar, K., Morlighem, M. & Gillet-Chaulet, F. Basal resistance for three of the largest Greenland outlet glaciers. *J. Geophys. Res. Earth* **121**, 168–180 (2016).
- Kehrl, L. M., Joughin, I., Shean, D. E., Floricioiu, D. & Krieger, L. Seasonal and interannual variability in terminus position, glacier velocity, and surface elevation at Helheim and Kangerlussuaq Glaciers from 2008 to 2016. *J. Geophys. Res. Earth* **122**, 1635–1652 (2017).
- Joughin, I., Smith, B. E., Howat, I. M., Scambos, T. A. & Moon, T. Greenland flow variability from ice-sheet-wide velocity mapping. *J. Glaciol.* **56**, 415–430 (2010).
- Howat, I. M. *MEaSURES Greenland Ice Velocity: Selected Glacier Site Velocity Maps from Optical Images, Version 1* (NASA, National Snow and Ice Data Center, Distributed Active Archive Center, Boulder, 2016).
- Morlighem, M., Rignot, E., Mouginot, J., Seroussi, H. & Larour, E. Deeply incised submarine glacial valleys beneath the Greenland ice sheet. *Nat. Geosci.* **7**, 418–422 (2014).
- Studinger, M. & IceBridge A. T. M. *L2 Icesat Elevation, Slope, and Roughness, Version 2* (NASA, National Snow and Ice Data Center, Distributed Active Archive Center, Boulder, 2017).
- Shreve, R. L. Movement of water in glaciers. *J. Glaciol.* **11**, 205–214 (1972).
- Howat, I. M., Negrete, A. & Smith, B. E. The Greenland Ice Mapping Project (GIMP) land classification and surface elevation data sets. *Cryosphere* **8**, 1509–1518 (2014).
- Kienholz, C., Hock, R. & Arendt, A. A. A new semi-automatic approach for dividing glacier complexes into individual glaciers. *J. Glaciol.* **59**, 925–937 (2013).
- Magorrian, S. J. & Wells, A. J. Turbulent plumes from a glacier terminus melting in a stratified ocean. *J. Geophys. Res. Oceans* **121**, 4670–4696 (2016).
- Holland, D. M. & Jenkins, A. Modeling thermodynamic ice–ocean interactions at the base of an ice shelf. *J. Phys. Oceanogr.* **29**, 1787–1800 (1999).